

# Plasmonic Cavity Formation by Circular and Spiral Corrugations

Kazuo OGURA, Yuta ANNAKA<sup>1)</sup>, Shin KUBO<sup>2)</sup> and Toru TSUJIMURA<sup>2)</sup>

*Graduate School of Science and Technology, Niigata University, Niigata 950-2181, Japan*

<sup>1)</sup>*Faculty of Engineering, Niigata University, Niigata 950-2181, Japan*

<sup>2)</sup>*College of Engineering, Chubu University, Kasugai 487-8501, Japan*

(Received 6 July 2022 / Accepted 31 December 2022)

Metal surfaces with sub-wavelength structures form a plasmon polariton-like surface mode, i.e., spoof-plasmon. The spoof-plasmon on a corrugated disk propagates radially and is reflected at the edge, resulting in formation of plasmonic cavity. With a concentric circular corrugation, the excited spoof-plasmons form an axisymmetric plasmonic cavity. With a spiral corrugation, the spoof-plasmons have non-zero orbital angular momenta and form a non-axisymmetric plasmonic cavity. Spoof-plasmons consisting of the plasmonic cavity transfer their angular momenta to radiation waves via the corrugated hollow waveguide by conserving their topological charges.

© 2023 The Japan Society of Plasma Science and Nuclear Fusion Research

Keywords: corrugated disk, deep corrugation, spoof-plasmon, plasmonic cavity, angular momentum, topological charge, spiral chirality

DOI: 10.1585/pfr.18.1406007

## 1. Introduction

Optical surface plasmon polariton (SPP) formed on material boundaries has orbital and spin angular momenta and its novel applications have been extensively studied in recent years [1, 2]. For example, angular momenta of SPP are controlled by corrugated structures on circular disks [3,4]. The SPPs excited propagate inwardly and outwardly along the disk surface, resulting in formation of plasmonic microcavity [5]. By using the cylindrical coordinate system  $(r, \varphi, z)$ , the  $z$ -component of the eigen mode on the disk may be expressed as,

$$E_z = E_0 J_m(k_r r) \exp[i(k_z z + m\varphi - \omega t)]. \quad (1)$$

Here,  $J_m$  is the  $m$ th order Bessel function of the first kind and  $m$  is the azimuthal mode number,  $E_0$  is a constant,  $k_z$  is the wavenumber perpendicular to the disk surface, and  $k_r$  is the radial wavenumber. Note that  $m$  corresponds to a normalized angular momentum and is referred to as a topological charge of SPP. A spiral structure of geometrical order  $l_s$  may give SPP a topological charge  $m = l_s$ , forming a plasmonic vortex with  $m$  [5].

Metamaterials like gratings or corrugated wall surfaces can form a surface wave which is mimicking the SPP and is called spoof-plasmon or spoof-SP [6, 7]. The spoof-plasmon is a surface wave extending along the metamaterial surface. A superior aspect of spoof-plasmon is that the dispersion characteristics can be artificially controlled by the structure. Therefore, physics and applications of surface-wave angular momentum in optics could be extended to the microwave and terahertz-wave regions [7]. For example, the spoof-plasmon is used in intense terahertz surface wave oscillators (SWOs) or backward wave

oscillators (BWOs) [8–10]. In real SWO devices, radiations with the azimuthal mode number  $m$  up to 30 are observed [11]. Hence, SWO is a very attractive candidate for generators of plasmonic vortex with large  $m$ . However, many spoof-plasmons having various  $m$  are generated simultaneously, resulting in a multimode operation. This is the well-known mode competition problem. To solve this problem, two-dimensional (2D) Bragg structures have been proposed to limit the operation to a small value of  $m$  [12]. This 2D structure has a doubly periodic corrugation in the longitudinal and transverse directions. The corrugations are shallow with the ratio of the corrugation depth to the period about 0.3, see Fig. 1. The SWO with such shallow corrugation should be driven by relativistic electron beams of about 300 keV or higher energy, because the operation is restricted to the Bragg resonance point, corresponding the  $\pi$ -point near the light velocity.

To use the asset of the spoof-plasmon, the spectrum needs to be widened away from the Bragg point, by deep-

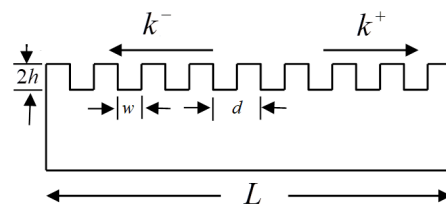


Fig. 1 Periodical corrugation with period  $d$ , amplitude  $h$ , and width  $w$ . The corrugation wavenumber is  $k_0 = 2\pi/d$ . The corrugation length  $L = Nd$  and  $N$  is the number of periods. Spoof-plasmons are formed and propagate with wavenumber  $k^-$  and  $k^+$  along the corrugation.

ening the corrugation. The deep corrugations have been successfully used for weakly relativistic SWOs with electron beams less than 100 keV [8–11, 13, 14]. In this case, axially forward and backward spoof-plasmons form an axial resonant cavity, which can strongly enhance terahertz-wave radiations. Thus, the operation based on the plasmonic cavity formation is very attractive for future intense terahertz-wave generators. However, it is still hard challenge to control  $m$  far from the Bragg point with deep corrugations.

In this paper, we examine plasmonic cavity on disks with circular and spiral corrugations. The corrugations are deep with the ratio of the corrugation depth to the period larger than 0.6, aiming at control of  $m$  far from the Bragg point. The plasmonic cavity generated by the deep corrugation are investigated by applying the cavity resonance method using a vector network analyzer (VNA).

## 2. Plasmonic Cavity on Periodic Corrugation

Figure 1 is a schematic of periodic corrugation with period  $d$ , amplitude  $h$  and width  $w$ . The corrugation wavenumber is defined as  $k_0 = 2\pi/d$ . We experimentally examine plasmonic cavities of corrugated disks like Fig. 2 (a) and compare with those of waveguide type corrugations like Fig. 2 (b). First, we briefly summarize the plasmonic cavity formation by the waveguide type corrugations having axially corrugated structures. According to the Floquet's theorem under the spatial periodicity in the  $z$ -direction, the dispersion curves of electromagnetic (EM) waves are periodic in the axial wavenumber ( $k_z$ ) space with a period of  $k_0 = 2\pi/d$ . Figure 3 shows dispersion curves of axisymmetric  $TM_{01}$  mode, in the first Brillouin zone ( $-k_0/2 \leq k_z \leq k_0/2$ ) based on the reduced-zone scheme. These dispersion curves are obtained using numerical methods presented in Refs. [15, 16]. For non-axisymmetric hybrid waveguide modes, the letters of EH and HE are often used. The definition is rather ambiguous. This paper follows the definition in Refs. [17–19]: the TE (TM) mode is dominant in the HE (EH) mode around  $k_z = 0$ . There is an upper cutoff at the  $\pi$ -point ( $k_z = \pm k_0/2$ ), where the normalized wavenumber is  $\pm 0.5$ . The dispersion curves are in the slow-wave region and the EM wave phase velocity is less than the light velocity. They are an artificial evanescent surface wave and are called spoof-plasmon. For the axial corrugation like Fig. 2 (b), the evanescent nature appears in the  $r$ -direction. The corrugation depth strongly affects the upper cutoff frequency. Deeply corrugated structures are essential for intense terahertz SWOs driven by weakly relativistic or non-relativistic electron beams [8–11, 13, 14].

A finite-length corrugation causes end's reflections and generates a forward ( $k^+$ ) and backward ( $k^-$ ) spoof-plasmons as shown in Fig. 3. They form standing waves (plasmonic cavities) satisfying the following relation for

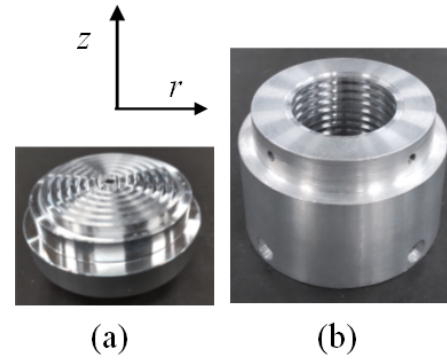


Fig. 2 Examples of periodically corrugated metals: (a) circular disk and (b) waveguide. The  $r$ - and  $z$ -axes of cylindrical coordinate system ( $r, \varphi, z$ ) are defined in the figure, where the  $\varphi$ -direction is defined according to the right-handed rule.

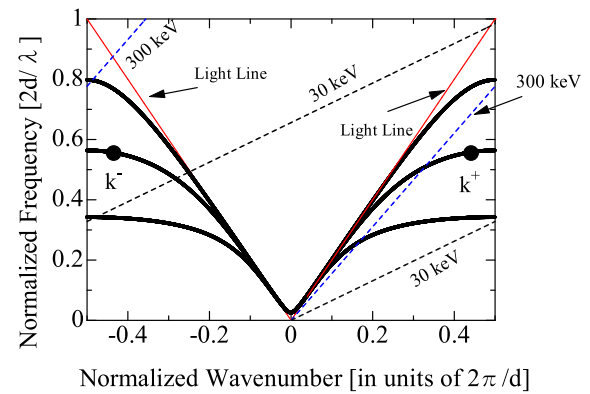


Fig. 3 Dispersion curves of axisymmetric  $TM_{01}$  mode in the periodically corrugated waveguide for intense terahertz SWOs, based on the reduced-zone scheme. The ratio of the corrugation depth to the corrugation period 0.3, 0.6, and 1.2, from the top. Solid thin lines (red) are light lines. Dotted lines are beams lines for 30 keV (black) and 300 keV (blue). Spoof-plasmons with wavenumber  $k^-$  and  $k^+$  propagating along the corrugation form a standing wave, i.e., a plasmonic cavity.

the angular frequency  $\omega$ .

$$\omega(k^+) = \omega(k^-). \quad (2)$$

Generally,  $k^+ = k^-$  and the plasmonic cavity at the upper cutoff may have a field pattern like Fig. 4 (a) [20–23]. The corresponding wavelength is  $\lambda_\pi = 2d$ . If both ends of cavity are strictly defined by metallic plates, amplitude of standing wave distributes like Fig. 4 (b) for a close-close cavity. Figure 4 (c) corresponds to an open-open cavity. In these cases, the wavenumber of plasmonic cavity may be given by,

$$k_r = \frac{\pi}{d} \times \frac{n}{N}. \quad (3)$$

Here,  $N$  is the number of corrugation periods, and  $n$  is integer ranging from 0 to  $N$ . For a practical case, ends are

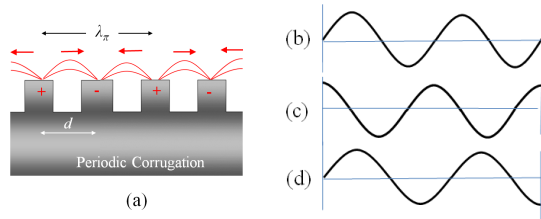


Fig. 4 (a) Field pattern of the  $\pi$ -point plasmonic cavity, (b), (c), and (d) are amplitude distributions of standing waves in short-short, open-open, and short-open cavities, respectively. (b) and (c) can satisfy the same boundary conditions on both ends. For (d), the boundary conditions on both ends differ and the standing wave is shifted by  $\lambda/4$  leading to the half-integer spacing, as mentioned in the main text. Here,  $\lambda$  is the wavelength.

not defined strictly and may have different conditions. For example, one end is open and the other one is close like Fig. 4 (d). Such a cavity has resonant modes with “a half-integer” spacing given by,

$$k_r = \frac{\pi}{d} \times \frac{n - 1/2}{N}, \quad (4)$$

with an integer  $n$  ranging from 1 to  $N$  [24].

Next, we discuss spoof-plasmons on a circular disk like Fig. 2 (a). For the corrugated disk, the evanescence of spoof-plasmon appears in the  $z$ -direction. The spoof-plasmons propagate in the  $r$ -direction, clinging to the disk surface. The radial functions of the spoof-plasmon are expressed by the Bessel functions [25]. The outgoing ( $k^+$ ) and incoming ( $k^-$ ) waves in Fig. 1 or 3 may be expressed by the Hankel function of the first kind  $H_m^{(1)}(k^+r)$  and second kind  $H_m^{(2)}(k^-r)$ , respectively. They can form a cylindrical standing wave expressed by the Bessel function of the first kind  $J_m(k_r r)$  with  $k_r = k^+ = k^-$ , like Eq. (1). To analyze plasmonic cavities formed by the radial standing wave, we assume the parallel dispersion characteristics to the axial corrugation case;

- (2.1) the corrugation in the  $r$ -direction generates the upper cutoff at the  $\pi$ -point of  $k_r = k_0/2 (= \pi/d)$
- (2.2) the radial wavenumbers of plasmonic cavity are quantized with equal intervals of  $\pi/d$ , just like the axial plasmonic cavities.

In the followings, the radial plasmonic cavities are examined experimentally by comparing with the dispersion characteristics of the spoof-plasmons that can be excited in the corrugated waveguide.

### 3. Plasmonic Cavity on Corrugated Disk

Figures 5 (a), (b), and (c) show flat-surface disk without a reflector and circularly corrugated disk without and with reflector, respectively. The corrugation parameters are

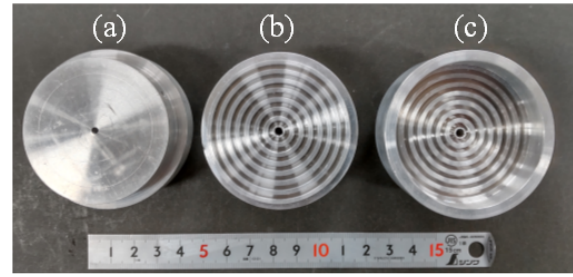


Fig. 5 Disks with (a) flat surface, (b) circular corrugation and (c) circular corrugation adding a reflector around the peripheral edge. They are made of aluminum and excited by a 1-mm needle antenna at the center. The radius of disk is  $R_0 = 26.0$  mm. The circular corrugations are concentric rings ( $l_s = 0$ ) and the number of circles is  $N = 7$ .

Table 1 Parameters of corrugations with deep corrugations.

$l_s$	$2h$ (mm)	$w$ (mm)	$d$ (mm)	$\Omega_{UC}^A$ (GHz)
0	2.4	1.7	3.4	23.0
1	2.2	1.5	3.0	25.3

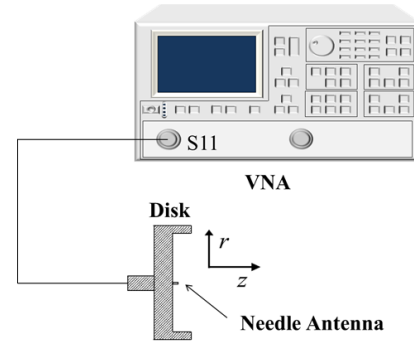


Fig. 6 Experimental setup for the single port measurement. Reflection ( $S_{11}$ ) from the disk is measured over the preset frequency range. The  $r$ - and  $z$ -axes of right-handed cylindrical coordinate system ( $r, \varphi, z$ ) are shown in the figure. The resonances appear as spikes of  $S_{11}$  at frequencies where the reflection is sharply reduced.

listed in Table 1. Numerically obtained upper cutoff frequencies  $\Omega_{UC}^A$  of waveguide type corrugation is also listed. The corrugations are deep with the depth  $2h/d$  of about 0.7. Plasmonic cavity formation is examined based on the cavity resonance method using an experimental setup shown in Fig. 6. Reflection  $S_{11}$  from the disk is measured as a function of frequency by using a VNA (Anritsu 37269D). Resonances due to the plasmonic cavity formation appear as spikes of  $S_{11}$ . Figure 7 (a) shows the experimental result for the flat disk. SPPs of aluminum surface are excited at the center and propagate outwardly. This outgoing SPP on the disk is expressed by the zero-order Hankel function of the first kind, which is given by superposing the outgo-

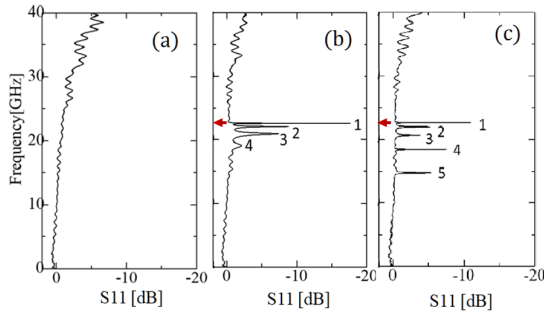


Fig. 7 Measured  $S_{11}$  profiles for (a) flat disk and (b) corrugated disk without reflector and (c) with the reflector. Red arrows in (b) and (c) indicate the upper cutoff at the  $\pi$ -point whose frequency is  $\Omega_{UC}^A$  in Table 1. The disks with  $l_S = 0$  in Figs. 5 (b) and (c) are used.

ing plane waves [25]. Since the measured  $S_{11}$  shows no spikes, reflectance of the outgoing SPP at the peripheral edge is too weak to form a plasmonic cavity.

In contrast to the flat disk, the corrugation on the disk produces plasmonic cavities even if there is no reflector as shown in Fig. 7 (b), where observed spikes are denoted as 1, 2, 3, and 4 from the top. By applying Eq. (3) with the open-open cavity assumed, these four resonances are plotted at  $k_r r_0 = 7\pi/7, 6\pi/7, 5\pi/7,$  and  $4\pi/7$  by filled circles in Fig. 8 (a). The upper cutoff frequency is that of the upper most resonance, which is 22.6 GHz. This is very close to  $\Omega_{UC}^A = 23.0$  GHz in Table 1, which is numerically obtained for the  $TM_{01}$  mode of the corrugated waveguide.

In the case of corrugated disk, incoming ( $k^-$ ) as well as outgoing ( $k^+$ ) spoof-plasmons are generated as schematically shown in Fig. 1 or 3. They cling to the corrugated surface and form standing waves without any reflector as shown in Fig. 7 (b). In Refs. [22,23], such a spoof-plasmon is named bounded surface wave. In Fig. 8 (a), the dispersion curve of axisymmetric  $TM_{01}$  mode for the axially corrugated waveguide is also plotted as a reference. This numerical curve coincides with the experimental data within 2%, and well represents the dispersion characteristics of the spoof-plasmon formed in the  $r$ -direction.

Figure 7 (c) is the result of the  $S_{11}$  measurement for the corrugated disk with a reflector around the outer edge of disk in Fig. 5 (c). Five spikes are observed and denoted by 1, 2, 3, 4, and 5. The boundary condition in this case may correspond to short at the reflector and open at the center. And, observed five resonances are plotted by open circles in Fig. 8 (a) according to Eq. (4) for the short-open cavity. Note that the plasmonic cavity at  $k_r d = (3-1/2)\pi/7$  (14.7 GHz) cannot be formed without the reflector and hence the spoof-plasmons in this region are not bounded surface waves. They are hybrid surface waves, which have the similar characteristics as SPPs of flat aluminum surface [6, 7]. Hence, resonance 5 in Fig. 7 (c) disappears if the reflector is removed like Fig. 7 (a).

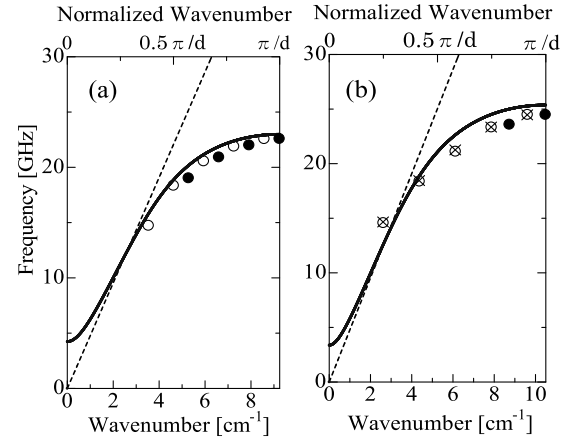


Fig. 8 Resonance frequencies obtained by the reflection measurement are plotted as a function of wavenumber for (a)  $l_S = 0$  and (b)  $l_S = 1$  and  $-1$ . The upper horizontal axes correspond to the normalized wavenumber. Since resonances are composed of waves with  $k^-$  and  $k^+$  as shown in Fig. 3, they are presented in the positive wavenumber region only ( $0 \leq k_r d \leq \pi$ ) with  $k = k^\pm$ . In (a), four filled circles correspond to four spikes of Fig. 7 (b), and five open circles correspond to five spikes of Fig. 7 (c). In (b), two filled circles correspond to two spikes of Fig. 10 (a) and five open circles (five crosses) correspond to five spikes of Fig. 10 (b) (Fig. 10 (c)). Solid curves in (a) and (b) are respectively the dispersion curves of axisymmetric  $TM_{01}$  mode and non-axisymmetric  $HE_{11}$  mode for the axially corrugated waveguide, which are obtained using numerical procedures presented in Refs. [15, 16] with the corrugation parameters listed in Table 1. Dotted lines are light lines.

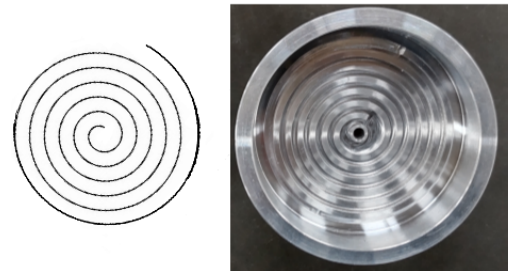


Fig. 9 Spiral disk of  $l_S = 1$ : (left) conceptual diagram and (right) photo of manufactured spiral with a reflector made of aluminum. It has six spirals,  $N = 6$ . The inner radius of reflector is  $R_0 = 26.0$  mm. The plus sign of  $l_S$  corresponds to the right-handed direction of the spiral looking from the top, which generates an incoming right-handed wave [4,5]. For excitation of outgoing right-handed wave, a reversed spiral with negative  $l_S$  should be used.

Next, we examine plasmonic cavities formed on the spiral disk. Figure 9 shows the spiral disk of  $l_S = 1$  with the reflector, which has the rotational number of six ( $N = 6$ ). Figures 10 (a) and (b) show the reflectance  $S_{11}$  measured as a function of frequency. Without the reflector,

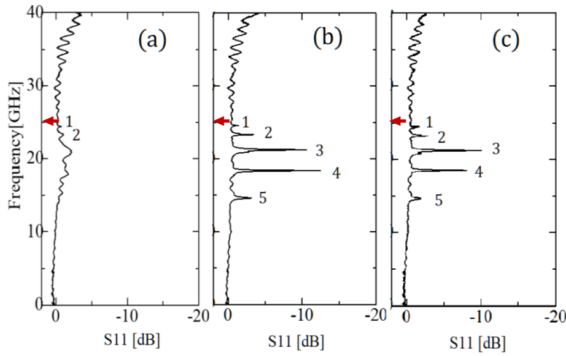


Fig. 10 Measured  $S_{11}$  profiles for the spiral disks: (a)  $l_S = 1$  without a reflector, (b)  $l_S = 1$  with a reflector, and (c)  $l_S = -1$  with a reflector. The frequencies at each resonance 1, 2, 3, 4 and 5 in (b) and (c) have almost the same values. Red arrows in (a), (b) and (c) indicate the upper cutoff at the  $\pi$ -point, whose frequency is  $\Omega_{UC}^A$  in Table 1.

very small  $S_{11}$  spikes denoted 1 and 2 are obtained near the  $\pi$ -point. These resonances are plotted at  $k_r d = 6\pi/6$  and  $5\pi/6$  by filled circles in Fig. 8 (b) by applying Eq. (3) with the open-open cavity assumed. With a reflector at the outer edge of disk, five resonances denoted by 1, 2, 3, 4, and 5 are observed as shown in Fig. 10 (b). They are plotted at  $k_r d = (6 - 1/2)\pi/6$ ,  $(5 - 1/2)\pi/6$ ,  $(4 - 1/2)\pi/6$ ,  $(3 - 1/2)\pi/6$ , and  $(2 - 1/2)\pi/6$  by open circles in Fig. 8 (b), according to Eq. (4) for the short-open cavity.

In Table 1,  $\Omega_{UC}^A = 25.3$  GHz for  $l_S = 1$  is a numerical upper cutoff frequency of the  $HE_{11}$  mode for the corrugated waveguide and is about 3% greater than the frequency of the uppermost resonance 1 of 24.5 GHz. The dispersion curve of the waveguide  $HE_{11}$  mode is also plotted in Fig. 8 (b) and well approximates the dispersion characteristics of the non-axisymmetric spoof-plasmon of the spiral disk.

#### 4. Angular Momentum of Spoof-Plasmon

To examine the angular momentum of spoof-plasmon, we measure the radiation patterns from a corrugated hollow waveguide excited by the disks as shown in Fig. 11 (a). The corrugation of the waveguide is axisymmetric and has no chirality like helical structures, and its parameters are the same as those for  $l_S = 1$  listed in Table 1. Radiation pattern from the waveguide is measured as angular distributions of the transmittance  $S_{21}$  by the VNA. A receiving horn antenna is moved on an equatorial plane around a pivot at the center of output of the waveguide. The distance between the antenna and the pivot is 600 mm. The electric fields are measured with the horizontal ( $\theta$ ) and vertical ( $\phi$ ) polarizations as defined in Fig. 11 (a), which are respectively denoted as  $E_\theta$  and  $E_\phi$ . Figure 11 (b) shows the radiation patterns with the disk of  $l_S = 0$ . The measured frequen-

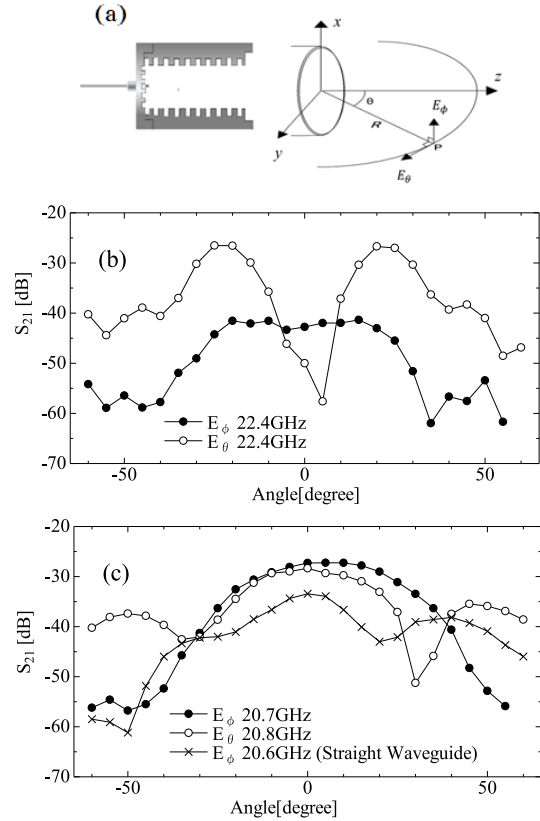


Fig. 11 (a) Experimental setup for radiation pattern measurement. The corrugated hollow waveguide is excited by a disk from the left side and radiation patterns are measured as  $S_{21}$  distribution with VNA from the right side. The corrugated hollow waveguide has parameters of  $2h = 2.2$  mm,  $d = 1.5$  mm, and  $z_0 = 3.0$  mm, which correspond to those for the 25.3 GHz upper cutoff in Table 1. Its averaged radius is 15.7 mm and periodic number is 10. (b) and (c) are the measured  $S_{21}$  with the disks of  $l_S = 0$  and  $-1$ , respectively. In (c), the radiation pattern replacing the corrugated hollow waveguide with a straight waveguide is also plotted.

cies are chosen as  $S_{21}$  takes a maximum value, and are near the upper cutoff of Figs. 7 (b) and (c). The radiation pattern is dominated by the axisymmetric  $TM_{01}$  mode. In Fig. 11 (c), the radiation patterns with the disk of  $l_S = -1$  are shown. The frequencies of maximum  $S_{21}$  are obtained near the resonance 3. In this case, the radiation patterns have a peak around the center, which can be explained by the  $TE_{11}$  component [26, 27].

Figure 12 shows angular distributions of  $S_{21}$  near the large resonances 3 (20.7 GHz) and 4 (17.8 GHz) in Figs. 10 (b) and (c). Near resonances, incoming and outgoing spoof-plasmons form cavities for both  $l_S = \pm 1$  spirals as shown in Fig. 10. And the outgoing spoof-plasmon couples to the waveguide. For the spiral disk with the reflector like Fig. 9, the reflection  $S_{11}$  is dominated by the plasmonic cavities only on the disk. On the other hand, the transmittance  $S_{21}$  in Figs. 11 and 12 is affected by the plas-

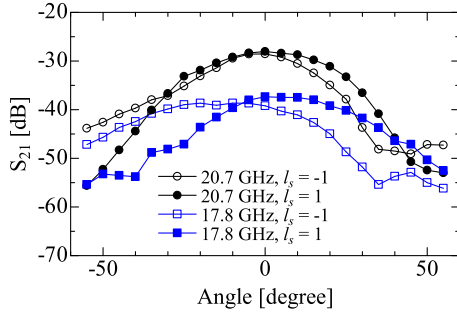


Fig. 12 Angular distributions of  $S_{21}$  with the spiral disks of  $l_S = -1$  and  $1$ . The same experimental setup of Fig. 11 (a) with the  $E_\phi$  polarity is used. Measured frequencies are 20.7 and 17.8 GHz, which respectively correspond the large resonances 3 and 4 in Figs. 10 (b) and (c).

monic cavities on the corrugated waveguide wall as well as on the disk. Note that spoof-plasmons are effectively generated in the bounded surface-wave region, which is above about 20 GHz for the corrugation waveguide used in Fig. 11 (a) [23]. Below the bounded surface-wave region, efficiency to excite spoof-plasmons on the waveguide wall may reduce resulting in a weak coupling between the disk and the waveguide. And hence,  $S_{21}$  at 17.8 GHz may become small compared with  $S_{21}$  at 20.7 GHz for both spirals with  $l_S = \pm 1$  in Fig. 12.

Relationship between topological charges of spoof-plasmon excited on the disk and the waveguide are considered. The topological charge is a normalized angular momentum, which consists of spin and orbit angular momentum [3–5, 28, 29]. The conservation law of angular momentum may be given by,

$$m_{Disk} = m_{WG}, \quad (5)$$

where  $m_{Disk}$  and  $m_{WG}$  are topological charges of the spoof-plasmon formed on the surfaces of the corrugated disk and the hollow corrugated waveguide, respectively. The  $m_{Disk}$  contains angular momenta generated by the spiral with  $l_S$ . For the disk with  $l_S = 0$ , the spoof-plasmon on the disk has  $m_{Disk} = 0$  and its zero-angular momentum is transferred to the corrugated waveguide. The corresponding spoof-plasmon of the corrugated waveguide is the axisymmetric  $TM_{01}$  mode with  $m_{WG} = 0$ , which is radiated from the waveguide and is observed as shown in Fig. 11 (b).

For the spiral disk with  $l_S = -1$ , the outgoing right-handed spoof-plasmon with  $m_{Disk} = 1$  is excited and couples to the non-axisymmetric mode with  $m_{WG} = 1$  in the corrugated waveguide. The corresponding spoof-plasmon of the waveguide is the  $HE_{11}$  mode. This mode may have a clockwise angular momentum corresponding to the  $l_S = -1$  spiral. When the corrugated waveguide is replaced by a straight waveguide, the peak value of  $S_{21}$  decreases by about 6 dB. This is attributed to the fact that no spoof-plasmon exists in the straight waveguide to accept the angular momentum from the disk. The volumetric  $TE_{11}$  and

$TM_{11}$  modes in the straight waveguide should be excited. In this case, the coupling between the disk and the waveguide becomes weak as shown in Fig. 11 (c).

## 5. Discussion and Conclusion

Here, we discuss the difference between the observed  $S_{11}$  behaviors of the disks with  $l_S = 0$  and  $\pm 1$ . For the concentric corrugation ( $l_S = 0$ ), the outgoing and incoming spoof-plasmons have  $m_{Disk} = 0$  and are respectively expressed by  $H_0^{(1)}(k^+r)$  and  $H_0^{(2)}(k^-r)$ . They form a standing wave expressed by  $J_0(kr)$  with  $k^\pm = k$ . In this case, the  $S_{11}$  spike becomes large as approaching the  $\pi$ -point like Figs. 7 (b) and (c). Since the  $S_{21}$  spikes becomes maximum near the upper cutoff of the spoof-plasmons with  $m_{Disk} = 0$ , the plasmonic cavities around this region can strongly couple to the waveguide mode.

On the other hand, the  $S_{11}$  spikes near the  $\pi$ -point are small for the spiral corrugation as shown in Figs. 10 (a) - (c). In Refs. [30–32], it is pointed out that spoof-plasmons attributed to helically corrugated wires have a distinctive chiral character, that is, the spoof-plasmon with the azimuthal mode number  $m$  has the following effective azimuthal mode number  $\tilde{m}$  near the  $\pi$ -point.

$$\tilde{m} \approx m + \frac{1}{2}. \quad (6)$$

Away from the  $\pi$ -point, this chirality is negligible and  $\tilde{m} \approx m$ . If this chirality effect appears in our spiral case of  $l_S = -1$  disk, the resonance 3 (21.1 GHz) in Fig. 10 (c), which is plotted at  $k_r = 0.58\pi/d$  in Fig. 8 (b), corresponds to the case apart from the  $\pi$ -point ( $k_r = \pi/d$ ). Its effective azimuthal mode number is  $\tilde{m} \approx m$ . The experiment shows that the spike is large, comparable to those of the disk with  $l_S = 0$ , for which there is no chirality effect. By approaching the  $\pi$ -point like resonance 1 in Fig. 10 (c), which is plotted at  $k_r = 0.92\pi/d$  in Fig. 8 (b), their effective azimuthal mode numbers may increase to  $\tilde{m} \approx 3/2$ . The corresponding  $S_{11}$  spike becomes very small indicating that the excitation efficiency of this mode is reduced. The same reduction of  $S_{11}$  is also observed by reversing the spiral direction, that is, using the spiral disk with  $l_S = 1$ , as shown in Fig. 10 (b). Our experiments show that the plasmonic cavity close to the  $\pi$ -point on the spiral disk couples poorly to the hollow corrugated waveguide. And the plasmonic cavity away from the  $\pi$ -point is used to maximize the  $S_{21}$ . Since mechanism causing the observed reduction of  $S_{11}$  and coupling efficiency to the waveguide is unresolved, the chirality effects of the spiral disk should be studied more definitely, by measuring EM field properties including the radial and azimuthal distributions.

In conclusion, plasmonic cavities formed on disks with circular and spiral corrugations are examined. Radially propagating spoof-plasmons are excited by a needle antenna at the center. The incoming as well as outgoing spoof-plasmons are generated due to the corrugation of the disk and the cylindrical plasmonic cavities are formed.

Their dispersion characteristics are parallel to those for the axial corrugation. When the disk has the concentric ring structure, the axisymmetric cavities are formed. If the disk has the spiral structure, the spoof-plasmons form the non-axisymmetric plasmonic cavities. These plasmonic cavities can excite the spoof-plasmon in the corrugated hollow waveguide. The angular momentum transferred from the disk to the hollow waveguide is ruled by the geometrical order of the disk. The control of angular momentum presented in this paper may be of considerable interest for applications in terahertz-wave as well as optics regions including a new intense terahertz-wave source.

## Acknowledgments

This work was partially supported by JSPS KAKENHI Grant Number JP22K14617 and by NIFS collaboration research program No. NIFS20KLER093. The authors would like to thank T. Takahashi (TDK Co. Ltd.) and S. Hamada (Honda Motor Co. Ltd.), for their contributions to the experiments.

- [1] K.Y. Bliokh *et al.*, Nat. Commun. **5**, 3300 (2014).
- [2] F. Cardano *et al.*, Nat. Photonics **9**, 776 (2015).
- [3] Y. Gorodetski *et al.*, Phys. Rev. Lett. **101**, 043903 (2008).
- [4] H. Kim *et al.*, Nano Lett. **10**, 529 (2010).
- [5] G. Spector *et al.*, Science **355**, 1187 (2017).
- [6] J.B. Pendry *et al.*, Science **305**, 847 (2004).
- [7] F.J. Garcia-Vidal *et al.*, Rev. Mod. Phys. **94**, 2 (2022).
- [8] S. Gong *et al.*, J. Appl. Phys. **118**, 123101 (2015).
- [9] M.T. Sun *et al.*, IEEE Trans. Plasma Sci. **45**, 30 (2017).
- [10] M.T. Sun *et al.*, IEEE Trans. Plasma Sci. **46**, 530 (2018).
- [11] Y. Annaka *et al.*, Phys. Plasmas **25**, 063115 (2018).
- [12] N.S. Ginzburg *et al.*, Phys. Rev. Accel. Beams **21**, 080701 (2018).
- [13] S. Aoyama *et al.*, Trans. Fusion Sci. Tech. **51**(2T), 325 (2007).
- [14] K. Ogura *et al.*, Plasma Fusion Res. **2**, S1041 (2007).
- [15] K. Ogura *et al.*, IEEE Trans. Plasma Sci. **44**, 201 (2016).
- [16] K. Ogura *et al.*, IEEE Trans. Plasma Sci. **49**, 40 (2021).
- [17] O. Watanabe *et al.*, Phys. Rev. E **63**, 056503 (2001).
- [18] H. Yamazaki *et al.*, J. Plasma Phys. **72**, 915 (2006).
- [19] H.-Z. Yao *et al.*, Opt. Commun. **354**, 401 (2015).
- [20] W. Main *et al.*, IEEE Trans. Plasma Sci. **22**, 566 (1994).
- [21] Md. R. Amin *et al.*, J. Phys. Soc. Jpn. **65**, 627 (1996).
- [22] K. Ogura *et al.*, Plasma Fusion Res. **7**, 2406022 (2012).
- [23] K. Ogura *et al.*, Plasma Fusion Res. **14**, 2406008 (2019).
- [24] S. Kobayashi *et al.*, IEEE Trans. Plasma Sci. **26**, 947 (1998).
- [25] R. Courant and D. Hirbert, *Methods of Mathematical Physics* (Wiley, New York, 1989), Vol. 2, Chap. 3.
- [26] S. Silver, *Microwave Antenna Theory and Design* (Mcgraw-Hill, New York, 1949).
- [27] P.J.B. Clarricoats and A.D. Olver, *Corrugated Horns for Microwave Antenna* (Peter Peregrinus, London, 1984).
- [28] Y. Gorodetski *et al.*, Nano Lett. **9**, 3016 (2009).
- [29] Y. Gorodetski *et al.*, Phys. Rev. Lett. **110**, 203906 (2013).
- [30] A.I. Fernández *et al.*, Appl. Phys. Lett. **93**, 141109 (2008).
- [31] S. Zhang *et al.*, Phys. Rev. Lett. **107**, 096801 (2011).
- [32] F. Ruting *et al.*, Phys. Rev. B **86**, 075437 (2012).